Letter

Clock-line photoassociation of strongly bound dimers in a magic-wavelength lattice

O. Bettermann,* N. Darkwah Oppong,† G. Pasqualetti,† L. Riegger, I. Bloch, and S. Fölling
Ludwig-Maximilians-Universität, Schellingstraße 4, 80799 München, Germany;
Max-Planck-Institut für Quantenoptik, Hans-Kopfermann-Straße 1, 85748 Garching, Germany;
and Munich Center for Quantum Science and Technology (MCQST), Schellingstraße 4, 80799 München, Germany

(Received 24 March 2020; accepted 5 June 2023; published 3 October 2023)

We report on the direct optical production and spectroscopy of $^1S_0$-$^3P_0$ molecules with large binding energy using the clock transition of ^{171}Yb, and on the observation of the associated orbital Feshbach resonance near 1300 G. We measure the magnetic field dependence of the closed-channel dimer and of the open-channel pair state energy via clock-line spectroscopy in a deep optical lattice. In addition, we show that the free-to-bound transition into the dimer can be made first-order insensitive to the trap depth by the choice of lattice wavelength. Finally, we determine the fundamental intra- and interorbital scattering lengths and probe the stability of the corresponding pair states, finding long lifetimes in both interorbital interaction channels. These results are promising both for molecular clocks and for the preparation of strongly interacting multiorbital Fermi gases.

DOI: 10.1103/PhysRevA.108.L041302

Alkaline-earth(-like) atoms (AEAs) such as ytterbium and strontium have attracted considerable interest in the field of ultracold atoms [1] due to their richer level structure compared to alkali metals. AEAs feature a long-lived $^3P_0$ state ($|e\rangle$) connected to the $^1S_0$ ground state ($|g\rangle$) via an ultranarrow clock transition, which is harnessed in today's most precise and accurate optical lattice clocks [2–5]. Moreover, the clock state provides an independent degree of freedom for quantum simulations of multiorbital many-body physics [6–16].

At the low energies and densities in these systems, interactions between atomic pairs are governed by their molecular interaction potential. In this regime, the properties of the bound states supported by this potential close to the dissociation energy threshold determine the scattering properties. In addition, if the energy of such a bound state can be suitably adjusted via a Zeeman shift, the interaction strength becomes precisely tunable with an external magnetic field. Such a mechanism lies at the heart of the magnetic Feshbach resonances utilized in alkali atoms [17]. In the case of an interorbital interaction potential, this leads to orbital Feshbach resonances (OFRs) [18], until now only observed in ^{173}Yb [19,20]. This type of Feshbach resonance allows tuning contact interactions between $|g\rangle$ and $|e\rangle$ atoms, and has enabled the realization of multiorbital Fermi polarons [13], coherent preparation of weakly bound dimers on the clock transition [21], and has inspired multiple proposals for the realization of exotic superfluidity [22–24].

The dimer state associated with the OFR in ^{173}Yb is weakly bound and intrinsically in the resonant regime, since its binding energy is comparable to other energy scales such as the band structure, the Fermi energy, or typical temperatures. Here, we report on a strongly bound molecular state in ^{171}Yb, outside the purely universal regime [25]. The binding energy of this molecule, while still close to the regime of a universal halo dimer, far exceeds all typical energy scales in cold atom ensembles. In particular, this also applies to the level spacing of the optical lattice traps typically used when driving the clock transition. The molecular wave function is therefore largely independent of the trap parameters, enabling a photoassociation process on a unique and particularly well-defined optical transition. This is especially promising in the context of molecular clocks, which have been proposed as sensitive probes for possible variations of fundamental constants and gravitation on microscopic scales [26–29]. Additionally, the OFR associated with the bound state in ^{171}Yb occurs at a large magnetic field where spin-exchange interactions are strongly suppressed by the differential Zeeman shift, in contrast to the OFR in ^{173}Yb [19].

We directly produce interorbital dimers in ^{171}Yb by addressing the narrow transition from pairs of weakly interacting $|g\rangle$ atoms to the least-bound molecular state in a deep three-dimensional (3D) optical lattice. First, we measure the energy of the dimer and of the repulsively interacting pair state at magnetic fields up to 1600 G. We find a large dimer binding energy of $h \times 292.1(2)$ kHz at zero magnetic field, in strong contrast with the very shallow bound state in ^{173}Yb [19], and the largest binding energies previously observed with photoassociation on doubly-forbidden transitions [30]. Our results are furthermore well described by a basic single-channel model corresponding to an OFR at 1300(44) G. In a second experiment, we show that the free-to-bound transition can be

*Oscar.Bettermann@physik.uni-muenchen.de
†These authors contributed equally to this work.

made first-order insensitive to the trap depth by adjusting the wavelength of the optical lattice, an essential step for the implementation of molecular clocks with this state. Furthermore, we precisely extract the intra- and interorbital scattering lengths via clock-line spectroscopy at small magnetic fields, finding values similar to the ones reported in Ref. [31]. Finally, we probe the stability of the corresponding eigenstates and find long-lived interorbital pair states, which are crucial for the implementation of many-body physics.

The characterization of the dimer and OFR in ^{171}Yb requires a detailed study of the magnetic-field-dependent interaction between two atoms in distinct orbitals ($|g\rangle$ or $|e\rangle$) and nuclear spin states ($m_F = \pm 1/2$, denoted by $|\uparrow\rangle$ and $|\downarrow\rangle$). At large magnetic fields B, the Hamiltonian is dominated by the differential Zeeman shift $|\delta(B)| = h \times 399.0(1)$ Hz/G $\times B/2$ [32] between $|g\uparrow\rangle$ and $|e\uparrow\rangle$ (or $|g\downarrow\rangle$ and $|e\downarrow\rangle$). At typical interparticle distances, the open channel $|o\rangle$ and closed channel $|c\rangle$ for the two-particle scattering problem are then given by $|eg\uparrow\downarrow\rangle = (|e\uparrow\rangle|g\downarrow\rangle - |g\downarrow\rangle|e\uparrow\rangle)/\sqrt{2}$ and $|eg\downarrow\uparrow\rangle = (|e\downarrow\rangle|g\uparrow\rangle - |g\uparrow\rangle|e\downarrow\rangle)/\sqrt{2}$, respectively. A free atomic pair entering $|o\rangle$ can couple to the least-bound state $|b_c\rangle$ supported by the closed-channel interatomic potential. This leads to an OFR when the corresponding molecular binding energy is offset by the differential Zeeman shift to the open channel, which changes the entrance energy by $\delta(B)$ [18].

In our experiment, we prepare a degenerate spin-balanced Fermi gas of ^{171}Yb in $|g\downarrow\rangle$ and $|g\uparrow\rangle$. We adiabatically load the atoms into a $30E_{\rm rec}$ deep and nearly isotropic 3D optical lattice operating at the magic wavelength $\lambda_m = 759.4$ nm [33], where atoms in $|g\rangle$ and $|e\rangle$ experience the same trapping potential. Here, $E_{\rm rec} = h \times 2.0$ kHz is the recoil energy of a lattice photon. The temperature is sufficiently low such that all atoms are in the motional ground state of each lattice site and ≈25% of the populated sites are doubly occupied.

We measure the transition energy to the dimer $|b_c\rangle$ and to the open-channel pair state $|o\rangle$ (which approaches the band excitation of the noninteracting system at large magnetic fields) for magnetic fields up to 1600 G, as shown in Figs. 1(a)–1(c). We directly drive on-site $|gg\rangle$ pairs to the desired interorbital state via the clock transition and measure the line shift compared to the $|g\uparrow\rangle \rightarrow |e\uparrow\rangle$ single-particle transition. Where the transition energies are above $-h \times 100$ kHz, we drive the dimer transition with long, low-intensity pulses while we use short, high-intensity pulses for lower energies. The open-channel state, and similarly the single-atom reference transition, are addressed with 5 ms coherent (Fourier-limited) pulses. The laser driving the clock transition is linearly polarized and propagating along one of the lattice axes. To reduce the effects of spatial inhomogeneity, we consider only a small region in the center of the atomic cloud, where ≈40% of the atoms are on doubly occupied lattice sites [32]. We obtain a transition energy of $-h \times 323.9(2)$ kHz at zero magnetic field, linearly extrapolating from the 1.1 G data point. We therefore obtain a molecular binding energy of $\epsilon_b = h \times 292.1(2)$ kHz, taking into account the difference in the harmonic oscillator ground state energies of the initial two-particle and final molecular states. With a separate measurement in pancake-shaped traps, we verify the production of the same molecules in a bulk gas [32]. The binding energy

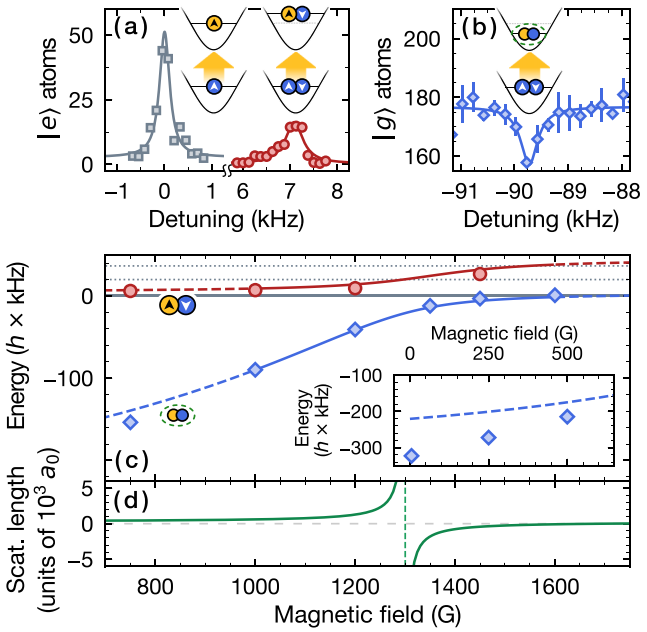

FIG. 1. Clock-line spectroscopy across the orbital Feshbach resonance. (a), (b) Raw spectra at 1000 G for the single-particle (gray squares), open-channel pair (red circles), and dimer (blue diamond) states. We use either the detection of $|e\rangle$ or $|g\rangle$ atoms to maximize the signal. The solid lines refer to Lorentzian fits and the error bars in (b) correspond to the standard error of two measurements. Blue (yellow) circles in the inset represent $|g\rangle$ ($|e\rangle$) atoms. (c) Energy of the open-channel pair state (red circles) and closed-channel dimer (blue diamonds) relative to the single-particle energy (solid gray line) at variable magnetic field. Data coinciding with the first or second band excitation (dotted gray lines) is not shown. In the inset, we show the dimer transition energy at small fields. We fit the data to our theoretical model between 1000 and 1600 G (solid lines), where the universal Feshbach relations hold well for the bound state. At other fields, we show the model as dashed lines. (d) Scattering lengths (solid line) and resonance position (dashed line) extracted from the fit in (c).

is much larger than all other energy scales in the system such as the temperature, the Fermi energy, or the lattice band gap, in stark contrast to the case of the near-resonant bound state in ^{173}Yb [19]. The dimer is therefore only weakly affected by the external confinement owing to the small size of its wave function. In the vicinity of the expected position of the OFR, between 1200 and 1450 G, we observe a strong loss of contrast on the transition to $|o\rangle$. At large fields above 1300 G, the binding energy vanishes as it approaches the threshold, a result of the diverging scattering length due to the OFR [see Fig. 1(d)].

To describe the above transition energies, we approximate each optical lattice site as a harmonic trap, allowing us to apply an analytic solution for the interacting atom pairs in our system [34]. We account for the lattice anharmonicity using first-order perturbation theory, in agreement with results from exact diagonalization in our regime [32,35,36]. Around the resonance, we use this model with the simple expression $a(B) = a_{\rm bg}[1 - \Delta/(B - B_0)]$ for the scattering length [17]. From this, we extract the position $B_0 = 1300(44)$ G, the width

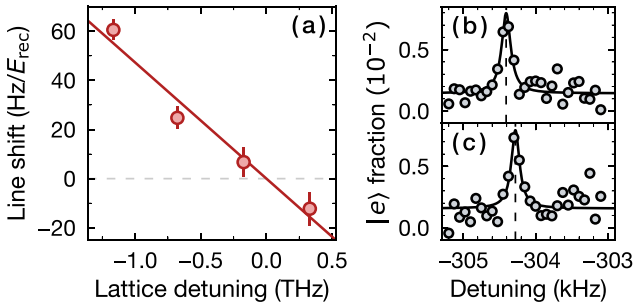

FIG. 2. Lattice-depth dependence of the free-to-bound transition at 1.1 G. (a) Linear shift of the transition relative to the lattice depth for varying detuning of the lattice laser. Each shift is determined from two consecutive measurements in a $25E_{rec}$ and $30E_{rec}$ deep lattice, with E_{rec} the photon recoil energy at the given lattice wavelength. The solid line corresponds to a linear fit and error bars denote the fit uncertainty of individual line shapes. The detunings are shown relative to the wavelength 776.6(3) nm [386.0(1) THz], which yields the first-order insensitive transition. (b), (c) Clock-line spectroscopy of the free-to-bound transition at 778 nm (385.3 THz) in a (b) $25.79(7)E_{rec}$ and (c) $30.95(8)E_{rec}$ deep lattice. The circles correspond to the fraction of $|e\rangle$ atoms and the solid line denotes a Lorentzian fit. We calculate the shift in (a) from both resonance positions (dashed lines)

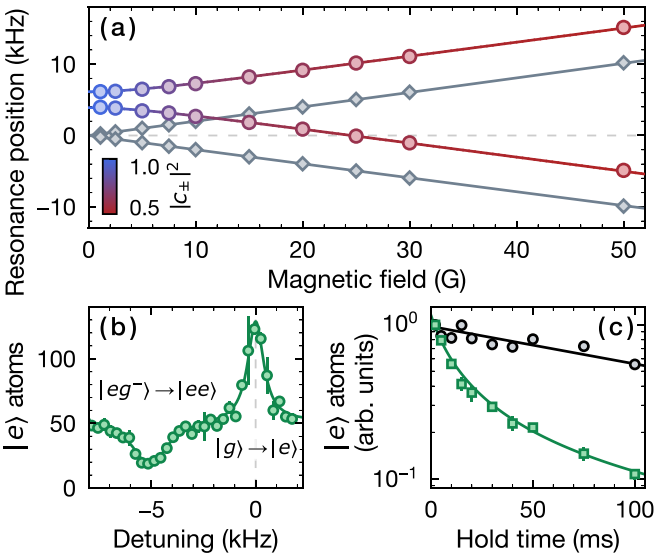

FIG. 3. Spectroscopy of pair states at low magnetic fields. (a) Transition energies to the $|eg\rangle$ pair eigenstates $|\psi^\pm\rangle$ (circles) as well as the $|e\uparrow\rangle$ and $|e\downarrow\rangle$ single-particle states (gray diamonds), compared to the zero-field single-particle transition (gray dashed line). Solid blue-red lines correspond to a fit of $E_\pm(B)$ from which we extract the corresponding scattering lengths. The color gradient reflects the overlap $|c_\pm|^2 = |\langle eg^\pm|\psi^\pm\rangle|^2$ of $|\psi^\pm\rangle$ with $|eg^-\rangle$ (upper branch) respectively $|eg^+\rangle$ (lower branch). The solid gray lines represent the differential Zeeman shift [32]. All data points are extracted from Lorentzian fits to spectroscopic measurements described in the main text. (b) Clock-line spectroscopy at 1.1 G of atom pairs in $|eg^-\rangle$. The solid line corresponds to a double Lorentzian fit, showing a loss feature at −5.1(1) kHz corresponding to the formation of $|ee\rangle$ pairs. (c) Lifetime of the $|ee\rangle$ state measured in a $31.2(8)E_{rec}$ deep single-axis optical lattice. We show the number $n(t)$ of remaining $|e\rangle$ atoms after varying hold time t in a spin-polarized (black circles) and spin-balanced sample (green squares). The solid lines denote fits to the data with an exponential decay (black) or a two-body decay $n(t) = n(0)/[1 + n(0)\beta_{ee}t]$ (green) [32].

$\Delta = 402(169)$ G, and the background scattering length $a_{bg} = 255(24)a_0$, where a_0 denotes the Bohr radius.

The deeply bound dimer produced in the above measurement is a promising candidate for the implementation of optical molecular clocks. The molecular line is however effectively broadened due to the inhomogeneous on-site trapping potential in the experiment. Compared to the single-atom wave function, the on-site molecular wave function is more localized and therefore experiences a larger average light intensity in a standing-wave optical lattice. This changes the effective polarizability of the molecule relative to the unbound state. We compensate this effect by introducing a suitable differential ac Stark shift between $|g\rangle$ and $|e\rangle$. This is achieved to first order by detuning the optical lattice from the magic wavelength of the single-particle transition. We note that the obtained wavelength is not universal, but specific to the selected magnetic field and lattice depth.

We explore this approach at a magnetic field $B = 1.1$ G by measuring how the free-to-bound transition line shifts between lattice depths of $25E_{rec}$ and $30E_{rec}$ for a range of lattice wavelengths λ_{lat} from 776 to 779 nm and observe a linear dependence of the line shift on λ_{lat}. We find that the transition frequency becomes independent of the lattice depth and the molecular line the narrowest for $\lambda_{lat} = 776.6(3)$ nm, as shown in Fig. 2. In the limit of zero magnetic field, the two-particle Hamiltonian is interaction dominated and its eigenstates are given by $|eg^+\rangle = (|eg\uparrow\downarrow\rangle - |eg\downarrow\uparrow\rangle)/\sqrt{2} = (|eg\rangle + |ge\rangle)/\sqrt{2} \otimes |s\rangle$ and $|eg^-\rangle = (|eg\uparrow\downarrow\rangle + |eg\downarrow\uparrow\rangle)/\sqrt{2} = (|eg\rangle - |ge\rangle)/\sqrt{2} \otimes |t\rangle$, connecting to $|o\rangle$ and $|c\rangle$ at large fields, respectively. Here, $|s\rangle$ denotes the nuclear spin singlet and $|t\rangle$ the nuclear spin triplet. In an optical lattice, the on-site interaction energies $U_{eg}^\pm$ directly depend on the corresponding scattering lengths $a_{eg}^\pm$, which contain fundamental information about the interorbital interactions of an $|eg\rangle$ pair.

We determine these scattering lengths with a spectroscopy technique similar to the one shown in Fig. 1. Here, we focus on low magnetic fields $\leqslant$50 G and measure the energy branches corresponding to $|eg^+\rangle$ as well as $|eg^-\rangle$ in the limit of zero magnetic field, the former connecting to the $|o\rangle$ branch in Fig. 1(c) at large fields. We apply high-resolution coherent clock pulses to couple the initial $|gg\rangle$ state to the desired state. In the spectra shown in Fig. 3(a), we identify two branches corresponding to the energies $E_\pm(B) - U_{gg}$ with respect to the single-particle transition energy at zero magnetic field. Here, U_{gg} is the magnetic-field-independent interaction of the initial $|gg\rangle$ pair. The magnetic field dependence of the energy branches at low fields is induced by the differential Zeeman shift $\delta(B)$ via $E_\pm(B) = V \pm \sqrt{V_{ex}^2 + \delta(B)^2}$ [37]. Here, $V = (U_{eg}^+ + U_{eg}^-)/2$ and $V_{ex} = (U_{eg}^+ - U_{eg}^-)/2$ denote the direct and spin-exchange energy, respectively. We adjust the Rabi frequency to compensate for the magnetic-field-dependent super- and subradiance of the pair states [32]. From these energies, we extract a_{eg}^+ as well as a_{eg}^- using a fit to a similar interaction

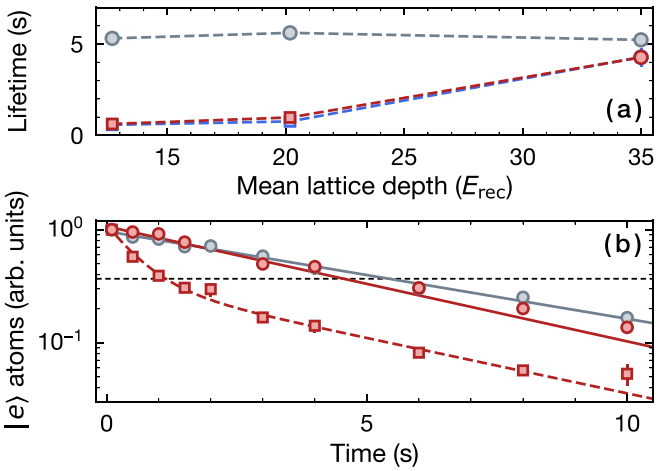

FIG. 4. Lifetime of the pair states in a 3D optical lattice. (a) Lifetime of $|eg^+\rangle$ (red) and $|eg^-\rangle$ (blue) states, compared to the lifetime of spin-polarized $|e\rangle$ atoms (gray). The dashed lines serve as a guide to the eye. We fit a sum of two exponentials (squares) or a single exponential (circles) to the atom number time traces. (b) Sample data and fits at $34.99(6)E_{\rm rec}$ (circles) respectively $20.18(5)E_{\rm rec}$ (squares) with sum of two exponentials (red dashed line) or single exponential fits (solid lines). The dashed horizontal line indicates the $1/e$ remaining fraction used to define the lifetime of the states.

model as for the OFR but with individual constant scattering lengths [32,34].

We find $a_{eg}^{+} = 240(4)a_0$ and $a_{eg}^{-} = 389(4)a_0$, where the initial-state interaction energy is determined by $a_{gg} = -2.8(3.6)a_0$ [38]. The error is dominated by the uncertainty in a_{gg} since the relative quantities $a_{eg}^{+} - a_{gg} = 242.7(1)a_0$ and $a_{eg}^{-} - a_{gg} = 392.2(2)a_0$ show an uncertainty smaller by an order of magnitude [32]. Crucially, these results imply that $V_{\rm ex} < 0$, corresponding to antiferromagnetic interorbital spin exchange, in qualitative agreement with a similar measurement [31]. The p-wave interaction in higher temperature ^{171}Yb gases has been previously analyzed in Ref. [39]. The presence of both ferromagnetic and antiferromagnetic exchange in ^{173}Yb [36,37] and ^{171}Yb, respectively, therefore enables the implementation of two-orbital Hamiltonians with either type of interaction.

To complete the characterization of all interaction channels, we measure the scattering length a_{ee} associated with a $|ee\rangle$ pair, which has not yet been determined in ^{171}Yb. With two consecutive excitation pulses, we drive atom pairs to $|eg^-\rangle$ and subsequently to $|ee\rangle$. When the second pulse is on resonance, we observe a loss of $|e\rangle$ atoms, as visible in Fig. 3(b). This is due to the short lifetime of on-site $|ee\rangle$ pair states, which is expected [6] and suggested by the broad loss feature. We extract $a_{ee} = 104(7)a_0$ from the spectral line using the same model as for the interorbital scattering lengths.

We additionally characterize the strongly inelastic collisions between two $|e\rangle$ atoms in a single-axis optical lattice at 30 G. Here, the confinement is reduced in order to decrease the density and make the experimental determination of the lifetime feasible. We employ two consecutive clock pulses much shorter than the $|ee\rangle$ lifetime addressing the single-particle transitions $|g\downarrow\rangle \rightarrow |e\downarrow\rangle$ and $|g\uparrow\rangle \rightarrow |e\uparrow\rangle$ to prepare the initial state and monitor the number of remaining $|e\rangle$ atoms for varying hold times [see Fig. 3(c)]. We find particularly short lifetimes and estimate a large effective two-body loss coefficient $\beta_{ee} = 4.8(2.1) \times 10^{-12}$ cm^3/s [32], which is comparable to a previous measurement with nondegenerate atoms [40]. The fast decay of the $|ee\rangle$ state highlights the importance to localize individual $|e\rangle$ atoms on lattice sites in quantum simulation experiments, which can be achieved with state-dependent optical lattices [10].

Finally, we probe the lifetimes of the interorbital pair states in a 3D optical lattice at 25 G. Long lifetimes of these states are essential for the study of multiorbital many-body physics. We prepare the pair states with high-intensity clock pulses and measure the decay with a second pulse after a variable hold time. In Fig. 4(a), we show the corresponding fits for different lattice depths and compare with the decay of $|e\uparrow\rangle$ atoms prepared in a spin-polarized sample. While the latter depends only weakly on the confinement, we find that the $|eg^{\pm}\rangle$ lifetimes are significantly reduced in shallower lattices. Since the $|g\rangle$ atom number remains constant, we conclude the losses are caused by residual tunneling of $|e\rangle$ atoms leading to the formation of short-lived $|ee\rangle$ pairs. In a $35E_{\rm rec}$ deep lattice, the observed lifetimes correspond to an inelastic loss-rate coefficient of $\beta_{eg}^{\pm} \leqslant 2.6(3) \times 10^{-16}$ cm^3/s [32]. We only specify an upper bound for $\beta_{eg}^{\pm}$ since our value also includes single-particle losses and effects of tunneling. Overall, the large observed $|eg^{\pm}\rangle$ lifetimes, longer than those reported in the high-temperature regime [40], are very suitable for implementations of two-orbital Hamiltonians with ^{171}Yb in state-dependent optical lattices.

In conclusion, we have directly produced and characterized deeply bound dimers in ^{171}Yb by addressing the narrow free-to-bound transition in a 3D optical lattice. Due to their large binding energy at zero magnetic field, these are only weakly perturbed by the external confinement, in stark contrast to ^{173}Yb. Moreover, we have determined the wavelength which makes the transition to the dimer state insensitive to the trap depth, providing a starting point for the state preparation in future molecular clock experiments. The OFR, which we find at a magnetic field about 1300 G, makes it an interesting system for exploring the rich physics of strongly interacting multiorbital quantum gases such as in the case of Fermi polarons [13]. Furthermore, we have precisely measured the interorbital scattering lengths, which imply antiferromagnetic spin-exchange interactions, in qualitative agreement with Ref. [31]. We also find low loss rates for interorbital atom pairs, making ^{171}Yb a promising platform for quantum simulations, in particular for Kondo impurity physics [11,12,14,15] and the Kondo lattice model [6–9].

We thank Jesper Levinsen and Meera M. Parish for insightful discussions. We also thank Florian Fertig and Caroline Tornow for technical contributions as well as the group of Gerhard Rempe for lending us equipment. This work was supported by the European Research Council through the synergy grant UQUAM and by the European Union's Horizon 2020 funding. N.D.O. acknowledges funding from the International Max Planck Research School for Quantum Science and Technology.

[1] C. He, E. Hajiyev, Z. Ren, B. Song, and G.-B. Jo, Recent progresses of ultracold two-electron atoms, J. Phys. B: At., Mol. Opt. Phys. **52**, 102001 (2019).

[2] A. D. Ludlow, M. M. Boyd, J. Ye, E. Peik, and P. O. Schmidt, Optical atomic clocks, Rev. Mod. Phys. **87**, 637 (2015).

[3] T. Takano, M. Takamoto, I. Ushijima, N. Ohmae, T. Akatsuka, A. Yamaguchi, Y. Kuroishi, H. Munekane, B. Miyahara, and H. Katori, Geopotential measurements with synchronously linked optical lattice clocks, Nat. Photonics **10**, 662 (2016).

[4] W. F. McGrew, X. Zhang, R. J. Fasano, S. A. Schäffer, K. Beloy, D. Nicolodi, R. C. Brown, N. Hinkley, G. Milani, M. Schioppo, T. H. Yoon, and A. D. Ludlow, Atomic clock performance enabling geodesy below the centimetre level, Nature (London) **564**, 87 (2018).

[5] T. Bothwell, D. Kedar, E. Oelker, J. M. Robinson, S. L. Bromley, W. L. Tew, J. Ye, and C. J. Kennedy, JILA SrI optical lattice clock with uncertainty of 2.0×10^{-18}, Metrologia **56**, 065004 (2019).

[6] A. V. Gorshkov, M. Hermele, V. Gurarie, C. Xu, P. S. Julienne, J. Ye, P. Zoller, E. Demler, M. D. Lukin, and A. M. Rey, Two-orbital $SU(N)$ magnetism with ultracold alkaline-earth atoms, Nat. Phys. **6**, 289 (2010).

[7] M. Foss-Feig, M. Hermele, and A. M. Rey, Probing the Kondo lattice model with alkaline-earth-metal atoms, Phys. Rev. A **81**, 051603(R) (2010).

[8] M. Foss-Feig, M. Hermele, V. Gurarie, and A. M. Rey, Heavy fermions in an optical lattice, Phys. Rev. A **82**, 053624 (2010).

[9] J. Silva-Valencia and A. M. C. Souza, Ground state of alkaline-earth fermionic atoms in one-dimensional optical lattices, Eur. Phys. J. B **85**, 5 (2012).

[10] L. Riegger, N. Darkwah Oppong, M. Höfer, D. R. Fernandes, I. Bloch, and S. Fölling, Localized magnetic moments with tunable spin exchange in a gas of ultracold fermions, Phys. Rev. Lett. **120**, 143601 (2018).

[11] M. Kanász-Nagy, Y. Ashida, T. Shi, C. P. Moca, T. N. Ikeda, S. Fölling, J. I. Cirac, G. Zaránd, and E. A. Demler, Exploring the anisotropic Kondo model in and out of equilibrium with alkaline-earth atoms, Phys. Rev. B **97**, 155156 (2018).

[12] M. Nakagawa, N. Kawakami, and M. Ueda, Non-Hermitian Kondo effect in ultracold alkaline-earth atoms, Phys. Rev. Lett. **121**, 203001 (2018).

[13] N. Darkwah Oppong, L. Riegger, O. Bettermann, M. Höfer, J. Levinsen, M. M. Parish, I. Bloch, and S. Fölling, Observation of coherent multiorbital polarons in a two-dimensional Fermi gas, Phys. Rev. Lett. **122**, 193604 (2019).

[14] S. Goto and I. Danshita, Quasiexact Kondo dynamics of fermionic alkaline-earth-like atoms at finite temperatures, Phys. Rev. Lett. **123**, 143002 (2019).

[15] R. Zhang and P. Zhang, Tight-binding Kondo model and spin-exchange collision rate of alkaline-earth-metal atoms in a mixed-dimensional optical lattice, Phys. Rev. A **101**, 013636 (2020).

[16] A. Sotnikov, N. Darkwah Oppong, Y. Zambrano, and A. Cichy, Orbital ordering of ultracold alkaline-earth atoms in optical lattices, Phys. Rev. Res. **2**, 023188 (2020).

[17] C. Chin, R. Grimm, P. Julienne, and E. Tiesinga, Feshbach resonances in ultracold gases, Rev. Mod. Phys. **82**, 1225 (2010).

[18] R. Zhang, Y. Cheng, H. Zhai, and P. Zhang, Orbital Feshbach resonance in alkali-earth atoms, Phys. Rev. Lett. **115**, 135301 (2015).

[19] M. Höfer, L. Riegger, F. Scazza, C. Hofrichter, D. R. Fernandes, M. M. Parish, J. Levinsen, I. Bloch, and S. Fölling, Observation of an orbital interaction-induced Feshbach resonance in ^{173}Yb, Phys. Rev. Lett. **115**, 265302 (2015).

[20] G. Pagano, M. Mancini, G. Cappellini, L. Livi, C. Sias, J. Catani, M. Inguscio, and L. Fallani, Strongly interacting gas of two-electron fermions at an orbital Feshbach resonance, Phys. Rev. Lett. **115**, 265301 (2015).

[21] G. Cappellini, L. F. Livi, L. Franchi, D. Tusi, D. Benedicto Orenes, M. Inguscio, J. Catani, and L. Fallani, Coherent manipulation of orbital Feshbach molecules of two-electron atoms, Phys. Rev. X **9**, 011028 (2019).

[22] M. Iskin, Two-band superfluidity and intrinsic Josephson effect in alkaline-earth-metal Fermi gases across an orbital Feshbach resonance, Phys. Rev. A **94**, 011604(R) (2016).

[23] P. Zou, L. He, X.-J. Liu, and H. Hu, Strongly interacting Sarma superfluid near orbital Feshbach resonances, Phys. Rev. A **97**, 043616 (2018).

[24] E. K. Laird, Z.-Y. Shi, M. M. Parish, and J. Levinsen, Frustrated orbital Feshbach resonances in a Fermi gas, Phys. Rev. A **101**, 022707 (2020).

[25] F. Ferlaino, S. Knoop, and R. Grimm, Ultracold Feshbach molecules, in *Cold Molecules: Theory, Experiment, Applications* (CRC Press, Boca Raton, FL, 2009), Chap. 9.

[26] T. Zelevinsky, S. Kotochigova, and J. Ye, Precision test of mass-ratio variations with lattice-confined ultracold molecules, Phys. Rev. Lett. **100**, 043201 (2008).

[27] S. Kotochigova, T. Zelevinsky, and J. Ye, Prospects for application of ultracold Sr_2 molecules in precision measurements, Phys. Rev. A **79**, 012504 (2009).

[28] M. Borkowski, Optical lattice clocks with weakly bound molecules, Phys. Rev. Lett. **120**, 083202 (2018).

[29] S. S. Kondov, C.-H. Lee, K. H. Leung, C. Liedl, I. Majewska, R. Moszynski, and T. Zelevinsky, Molecular lattice clock with long vibrational coherence, Nat. Phys. **15**, 1118 (2019).

[30] S. Kato, S. Sugawa, K. Shibata, R. Yamamoto, and Y. Takahashi, Control of resonant interaction between electronic ground and excited states, Phys. Rev. Lett. **110**, 173201 (2013).

[31] K. Ono, J. Kobayashi, Y. Amano, K. Sato, and Y. Takahashi, Antiferromagnetic interorbital spin-exchange interaction of ^{171}Yb, Phys. Rev. A **99**, 032707 (2019).

[32] See Supplemental Material at http://link.aps.org/supplemental/10.1103/PhysRevA.108.L041302 for additional information about the experimental methods and theoretical modeling, which includes Refs. [41–50].

[33] N. D. Lemke, A. D. Ludlow, Z. W. Barber, T. M. Fortier, S. A. Diddams, Y. Jiang, S. R. Jefferts, T. P. Heavner, T. E. Parker, and C. W. Oates, Spin-1/2 optical lattice clock, Phys. Rev. Lett. **103**, 063001 (2009).

[34] T. Busch, B.-G. Englert, K. Rzażewski, and M. Wilkens, Two cold atoms in a harmonic trap, Found. Phys. **28**, 549 (1998).

[35] F. Deuretzbacher, K. Plassmeier, D. Pfannkuche, F. Werner, C. Ospelkaus, S. Ospelkaus, K. Sengstock, and K. Bongs, Heteronuclear molecules in an optical lattice: Theory and experiment, Phys. Rev. A **77**, 032726 (2008).

[36] G. Cappellini, M. Mancini, G. Pagano, P. Lombardi, L. Livi, M. Siciliani de Cumis, P. Cancio, M. Pizzocaro, D. Calonico, F. Levi, C. Sias, J. Catani, M. Inguscio, and L. Fallani, Direct

observation of coherent interorbital spin-exchange dynamics, Phys. Rev. Lett. **113**, 120402 (2014).

[37] F. Scazza, C. Hofrichter, M. Höfer, P. C. De Groot, I. Bloch, and S. Fölling, Observation of two-orbital spin-exchange interactions with ultracold SU(N)-symmetric fermions, Nat. Phys. **10**, 779 (2014).

[38] M. Kitagawa, K. Enomoto, K. Kasa, Y. Takahashi, R. Ciuryło, P. Naidon, and P. S. Julienne, Two-color photoassociation spectroscopy of ytterbium atoms and the precise determinations of s-wave scattering lengths, Phys. Rev. A **77**, 012719 (2008).

[39] N. D. Lemke, J. von Stecher, J. A. Sherman, A. M. Rey, C. W. Oates, and A. D. Ludlow, p-wave cold collisions in an optical lattice clock, Phys. Rev. Lett. **107**, 103902 (2011).

[40] A. D. Ludlow, N. D. Lemke, J. A. Sherman, C. W. Oates, G. Quéméner, J. von Stecher, and A. M. Rey, Cold-collision-shift cancellation and inelastic scattering in a Yb optical lattice clock, Phys. Rev. A **84**, 052724 (2011).

[41] J. R. de Laeter and N. Bukilic, The isotopic composition and atomic weight of ytterbium, Int. J. Mass Spectrom. **252**, 222 (2006).

[42] G. Pasqualetti, Isotopic mixtures of ytterbium for quantum simulation of Kondo physics, Master's thesis, LMU München, 2018.

[43] H. Katori, M. Takamoto, V. G. Pal'chikov, and V. D. Ovsiannikov, Ultrastable optical clock with neutral atoms in an engineered light shift trap, Phys. Rev. Lett. **91**, 173005 (2003).

[44] G. Reinaudi, T. Lahaye, Z. Wang, and D. Guéry-Odelin, Strong saturation absorption imaging of dense clouds of ultracold atoms, Opt. Lett. **32**, 3143 (2007).

[45] J. E. Sansonetti and W. C. Martin, Handbook of basic atomic spectroscopic data, J. Phys. Chem. Ref. Data **34**, 1559 (2005).

[46] M. M. Boyd, T. Zelevinsky, A. D. Ludlow, S. Blatt, T. Zanon-Willette, S. M. Foreman, and J. Ye, Nuclear spin effects in optical lattice clocks, Phys. Rev. A **76**, 022510 (2007).

[47] N. D. Lemke, Optical lattice clock with spin-1/2 ytterbium atoms, Ph.D. thesis, University of Colorado, Boulder, 2012.

[48] V. V. Flambaum, G. F. Gribakin, and C. Harabati, Analytical calculation of cold-atom scattering, Phys. Rev. A **59**, 1998 (1999).

[49] F. Scazza, Probing SU(N)-symmetric orbital interactions with ytterbium Fermi gases in optical lattices, Ph.D. thesis, LMU München, 2015.

[50] J. J. García-Ripoll, S. Dürr, N. Syassen, D. M. Bauer, M. Lettner, G. Rempe, and J. I. Cirac, Dissipation-induced hard-core boson gas in an optical lattice, New J. Phys. **11**, 013053 (2009).